

# Spherical Wave AVO Modelling of Converted Waves in Elastic Isotropic Media

Arnim B. Haase, CREWES, The University of Calgary, Calgary



2004 CSEG National Convention

## Summary

The AVO-response of two layer elastic and isotropic models for AVO-Classes 1 and 3 is investigated for converted waves. Zoeppritz's reflection coefficients and the Weyl-integral are utilized for the computations. Spherical wave results for  $R_{ps}$  and  $R_{pp}$  are compared with plane wave reflectivity. Depth dependence of spherical wave AVO is found to be strongest near critical angles of Class 1. Phase rotation is also observed under these conditions. There is some similarity between  $R_{ps}$  and  $R_{pp}$  for Class 1. Normalized Class 3 responses show no depth dependence. There is no similarity between Class 3  $R_{ps}$  and  $R_{pp}$ .

## Introduction

AVO-analysis and AVO-inversion are widely accepted tools in seismic exploration. The common approach is plane-wave analysis and linear approximations of the Zoeppritz equations are utilized to this end. For these approximations small incidence angles and small parameter changes are assumed. In recent years three parameter AVO-inversion has been investigated for the extraction of density information (e.g. Downton and Lines, 2001, as well as Kelly and Skidmore, 2001). It was observed that for reasonably accurate density estimates larger offsets/angles are required than normally used for two parameter inversion, preferably even postcritical events if present. Linearized approximations begin to break down at larger angles and are not applicable near critical points. Even "exact Zoeppritz" is a plane wave approximation to the real world. Winterstein and Hanten (1985) show that cylindrical wave modeling results in a much better fit of seismic data than does plane wave modeling near critical angles. Instead of the amplitude jump at the critical angle predicted by plane-wave theory, they find a more gradual amplitude transition for cylindrical wave models and actual data. In order to increase the accuracy of AVO-inversion, joint PP-PSv inversion has been suggested and investigated (see for example Margrave et al., 2001). The question arises as to what the spherical wave AVO-response of converted waves might be. This modelling study attempts to provide some answers to this question and investigates the spherical wave AVO-response of converted waves for AVO-Classes 1 and 3.

## Theory

Plane-wave particle motion reflection and transmission coefficients for elastic isotropic media in welded contact are given by Zoeppritz's equations. The formalism for expressing spherical wave fronts as contour integrals over plane waves goes back to Weyl (1919). Aki and Richards (1980, p217) derive equations for generalized PP-reflections and generalized PSv-reflections in terms of potentials  $\Phi$  (Equation 1) and  $\Psi$  (Equation 2):

$$\Phi = Ai\omega e^{-i\omega t} \int_0^{\infty} R_{pp} \frac{p}{\xi} J_0(\omega pr) e^{i\omega \xi(z+h)} dp \quad (1), \quad \Psi = Ai\omega e^{-i\omega t} \int_0^{\infty} \left( \frac{1}{i\omega p} \frac{\beta}{\alpha} R_{ps} \right) \frac{p}{\xi} J_0(\omega pr) e^{i\omega(\xi h + \eta z)} dp \quad (2)$$

Reflections from an elastic interface are computed firstly by introducing particle motion reflection coefficients given by Zoeppritz's equations. Secondly, particle motion  $u$  is computed from Equation (3)

$$u = \nabla\Phi + \nabla \times \nabla \times (0,0,\Psi) \quad (3)$$

and from the potentials given by Equations (1) and (2). Thirdly, normalization by the incident spherical P-wave particle motion leads to the spherical wave PP and PSv reflection coefficients. The integrations shown in Equations (1) and (2) proceed one frequency point at a time. When all frequency points are computed for the desired output bandwidth, the time domain response is found by inverse Fourier transform. Quadrature traces are determined by Hilbert transform. From these two trace types amplitude and phase of reflected spherical waves are calculated.

## Modelling

An actual gas-sand reservoir from the prairies is utilized to derive two layer models for this study. Density  $\rho_1$  is 2400 kg/m<sup>3</sup> for the layer just above the reservoir. P-wave velocity  $\alpha_1 = 2000$  m/s is dictated by a reservoir depth of 500m and a corresponding two-way travel-time of approximately 500ms. The layer parameters for AVO-Classes 1 and 3 shown in Table1 are adapted from Rutherford and Williams (1989).

Table 1:

Class	$\alpha_1$ /[m/s]	$\beta_1$ /[m/s]	$\rho_1$ /[kg/m <sup>3</sup> ]	$\alpha_2$ /[m/s]	$\beta_2$ /[m/s]	$\rho_2$ /[kg/m <sup>3</sup> ]
1	2000	879.88	2400	2933.33	1882.29	2000
3	2000	879.88	2400	1963.64	1260.04	2000

Output signal bandwidth and linear edge tapers are determined by choosing a 5/15-80/100 Hz Ormsby wavelet as the source signature. Free surface effects are not considered in this study. A P-wave point source and spherical wave fronts are assumed for the computations. All resulting spherical wave reflection amplitudes are normalized to zero-offset plane wave PP reflection coefficients in addition to an incident spherical P-wave normalization. AVO-Class 1 comparisons are shown in Figures 1, 2 and 3. Figure 1a displays normalized spherical wave PSv-reflection traces. Figure 1b gives a PP-reflection comparison. Figures 2a and 2b show the AVO-response magnitudes computed from these reflection traces. In Figures 3a and 3b the corresponding AVO-Class 1 phase responses can be seen. Similarly, AVO-Class 3 results are shown in Figures 4 and 5. Plane wave comparisons are added to all AVO magnitude and phase responses in order to highlight the impact of spherical wave fronts.

## Discussion and Conclusions

For Class 1 AVO-models, P-wave and S-wave velocities are increasing across the interface as can be seen in Table1. Because of this velocity increase critical angles exist and head waves are generated in Class 1 models. A head wave can be seen separating from reflected waves at the highest angles in Figure 1a. It also exists in Figure 1b but is not as evident for the angles shown. Note that the trace displays in Figures 1a, 1b, 4a and 4b are scaled individually in order to accommodate maximum amplitudes. The PSv-reflection traces in Figure 1a start with zero amplitude at zero angle. Then a negative reflection (-180 degrees of angle) grows stronger towards a magnitude maximum just below 30 degrees. Beyond 30 degrees the PSv-reflection strength diminishes first and then goes through a 90 degree phase rotation and increasing strength near the critical angle just beyond 40 degrees. With angles increasing beyond that, amplitudes diminish towards zero at 90 degrees and the phase angle returns to -180 degrees. Figure 2a shows the magnitude of  $R_{ps}$  for Class 1. The greatest departure from a plane wave comparison is observed in the vicinity of the critical angle. The larger the reflector depth, the closer the spherical response to the plane wave comparison; however, even at 2000m depth, there are significant differences. The Class 1 phase angle of  $R_{ps}$  is plotted in Figure 3a. Wrap around is dealt with by sign change. The considerable numerical jitter is assumed to be caused by time sampling of the reflectivity traces. The shallower the reflector, the more departure of the phase response from a plane wave comparison is found, similar to the magnitude response in Figure 2a. In both cases, Figures 2a and 3a, the response moves to larger angles with decreasing reflector depth and also spreads over a wider angle range. The Class 1 PP-reflection comparisons in Figures 1b, 2b and 3b bear striking similarities to their PSv counterparts in the way they differ from plane wave behavior near the critical angle. The depth dependence of spherical wave Class 1 AVO-responses of  $R_{ps}$  and  $R_{pp}$  is quite similar, including the phase rotation near the critical angle.

Results of AVO-Class 3 modelling are very different when compared to Class 1. Table 1 shows a P-wave velocity inversion, only S-wave velocities increase across the interface. There is no head wave and no phase rotation because there is no critical angle for incident P-waves. Another interesting observation is the apparent lack of depth dependence. The reasons for this apparent depth independence of Class 3 spherical wave AVO-responses are firstly the normalization and secondly the equal angle displays. Away from the critical angle the Class 1 response is also increasingly independent of depth. Class 3  $R_{ps}$  in Figures 4a and 5a starts off from zero and turns negative first, as before in Figure 1a. By contrast to Class 1, it goes through zero at about 60 degrees of angle and turns positive. Similar to Class 1  $R_{ps}$ , reflection strength returns to zero when approaching 90 degrees. Significant departure from a plane wave comparison occurs only above approximately 65 degrees for Class 3  $R_{ps}$ . The Class 3 PP-reflection (Figure 4b) is always negative and nonzero for any angle. Class 3  $R_{pp}$  (Figure 5b) departs significantly from a plane wave comparison between approximately 15 degrees and 75 degrees of angle. There is no apparent similarity between Class 3  $R_{ps}$  and  $R_{pp}$ .

The above spherical wave results are obtained by numerical integration. Krail and Brysk (1983) suggest a plane wave correction factor approximation for spherical waves. It will be interesting to compare the two approaches.

## References

- Aki, K.T., and Richards, P.G., 1980, Quantitative Seismology: Theory and Methods: Vol. 1, W.H. Freeman and Co.
- Downton, J.E., and Lines, L.R., 2001, Constrained Three parameter AVO inversion and uncertainty analysis: 71<sup>st</sup> Ann. SEG Mtg., Expanded Abstracts, 251-254.
- Kelly, M.C., and Skidmore, C., 2001, Non-linear AVO equations and their use in three parameter inversions: 71<sup>st</sup> Ann. SEG Mtg., Expanded Abstracts, 255-256.
- Krail, P.M., and Brysk, H., 1983, Reflection of spherical seismic waves in elastic layered media; Geophysics, **48**, 655-664.
- Margrave, G.F., Stewart, R.R., and Larsen, J.A., 2001, Joint PP and PS seismic inversion: The Leading Edge, **20**, no. 9, 1048-1052.
- Rutherford, S.R., and Williams, R.H., 1989, Amplitude-versus-offset variations in gas sands: Geophysics, **54**, 680-688.
- Weyl, H., 1919, Ausbreitung elektromagnetischer Wellen ueber einem ebenen Leiter: Ann. Physik, **60**, 481-500.
- Winterstein, D.F., and Hanten, J.B., 1985, Supercritical reflections observed in P- and S-wave data: Geophysics, **50**, 185-195.

## Acknowledgements

Thank you to Professor E. Krebs and Dr. C. Ursenbach for their help with the theory. Support by the CREWES team and its industrial sponsorship is gratefully acknowledged.

Fig.1a: Class 1 Spherical Wave PS Reflection (z=500m)

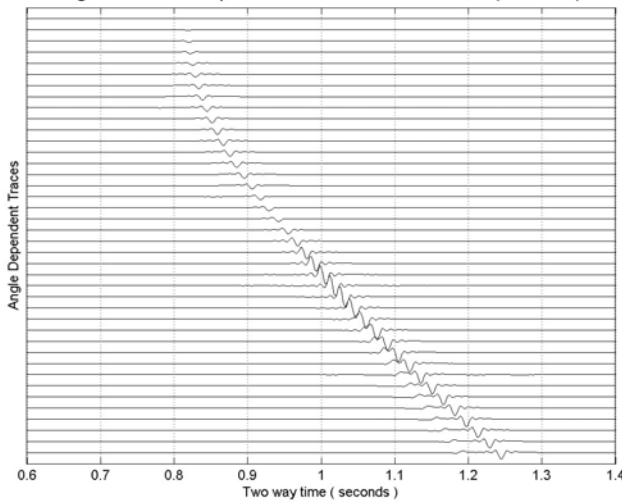


Fig.1b: Class 1 Spherical Wave PP Reflection (z=500m)

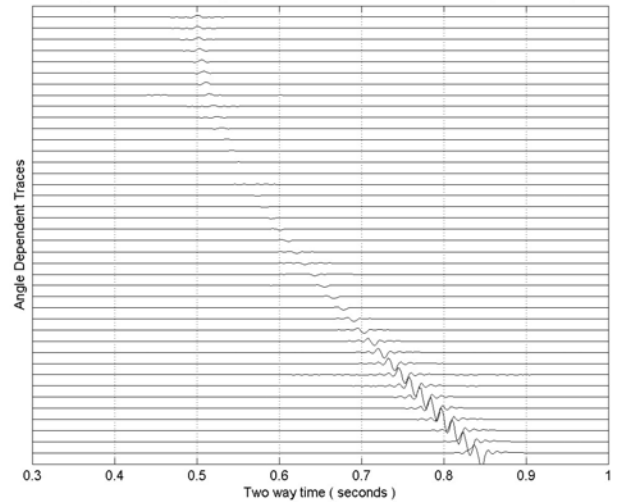


Fig.2a: AVO-Class 1 Spherical Wave PS Reflection Coefficient

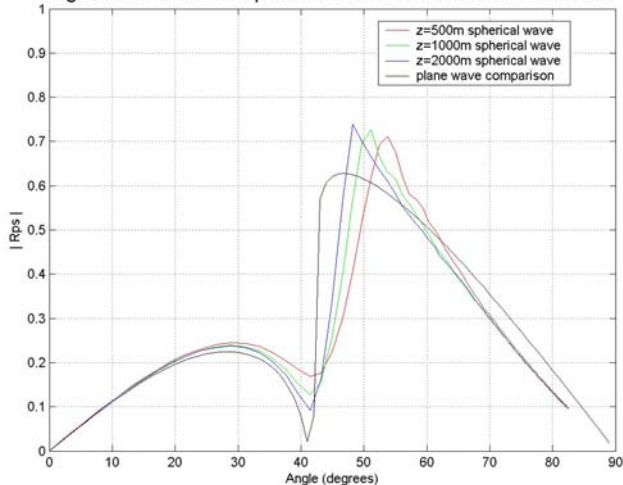


Fig.2b: AVO-Class 1 Spherical Wave PP Reflection Coefficient

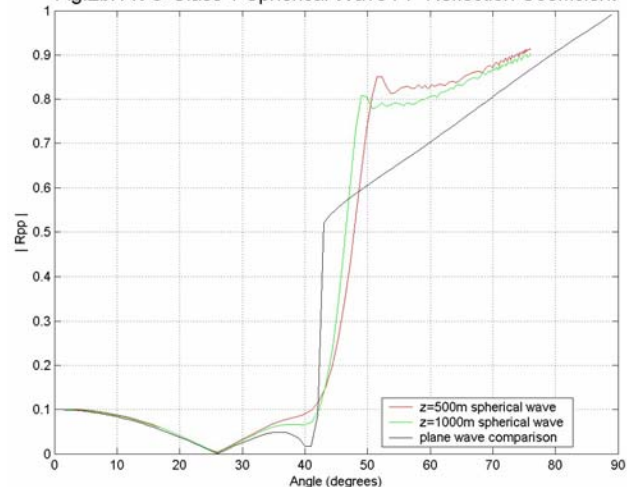


Fig.3a: AVO-Class 1 Spherical Wave PS Reflection Phase Angle

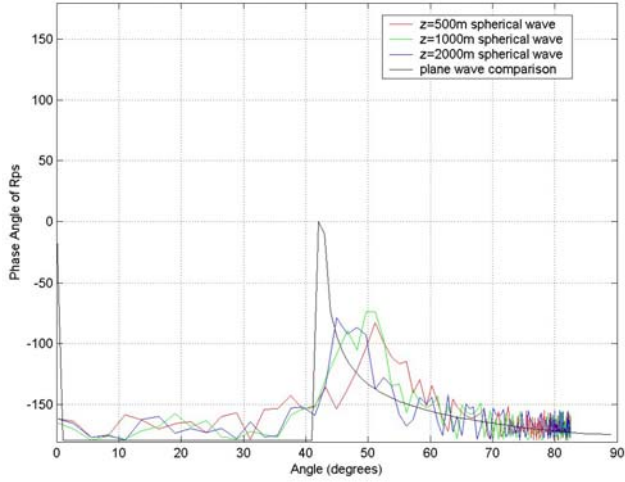


Fig.3b: AVO-Class 1 Spherical Wave PP Reflection Phase Angle

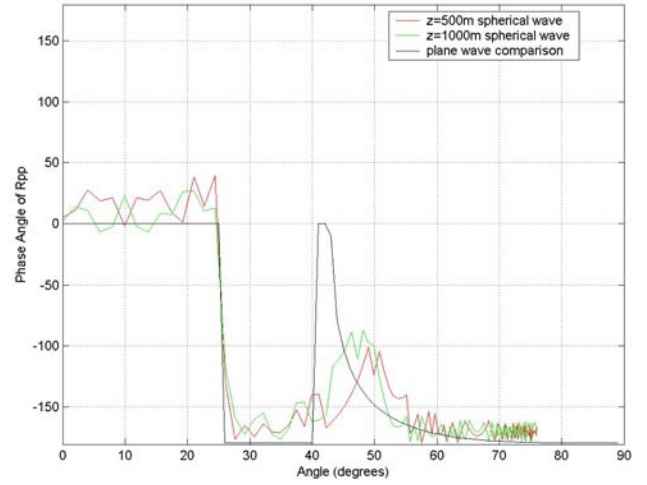


Fig.4a: Class 3 Spherical Wave PS Reflection (z=500m)

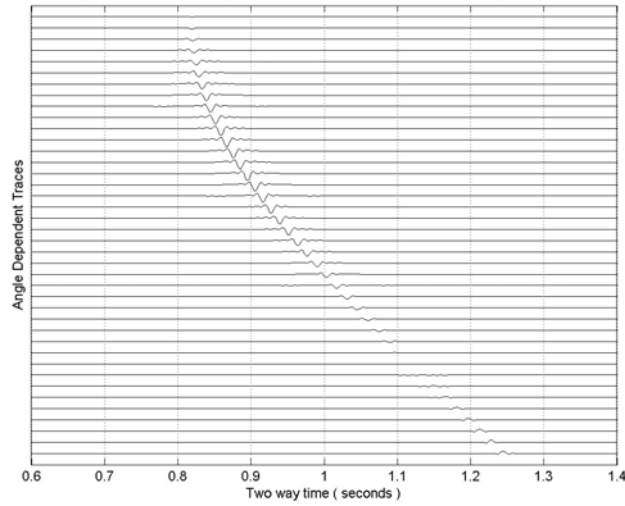


Fig.4b: Class 3 Spherical Wave PP Reflection (z=500m)

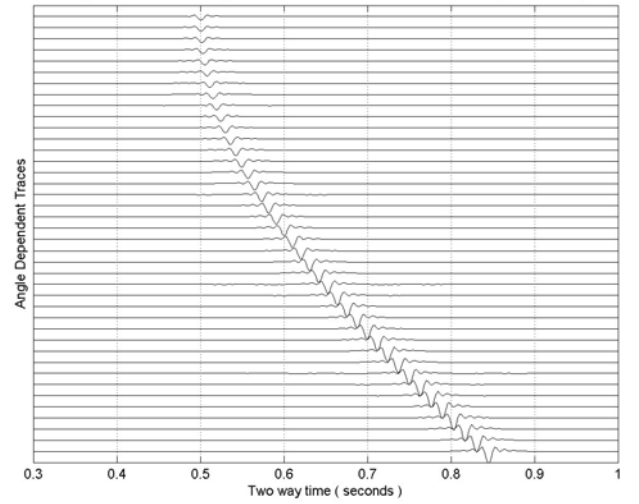


Fig.5a: AVO-Class 3 Spherical Wave PS Reflection Coefficient

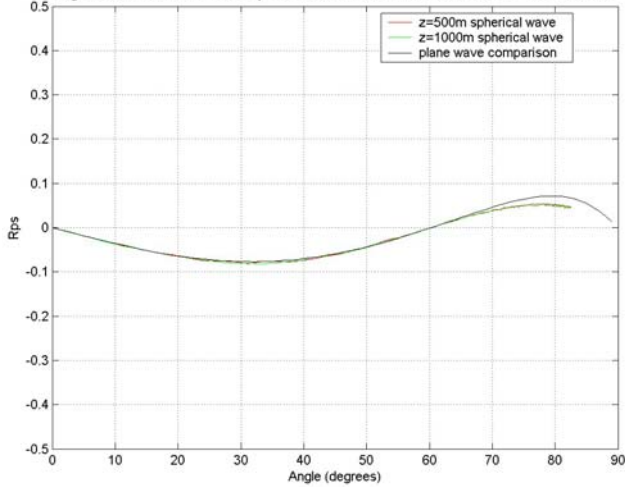


Fig.5b: AVO-Class 3 Spherical Wave PP Reflection Coefficient

